Efficient filter for detecting gravitational wave bursts in interferometric detectors

Thierry Pradier, Nicolas Arnaud, Marie-Anne Bizouard, Fabien Cavalier, Michel Davier, and Patrice Hello
Laboratoire de l'Accélérateur Linéaire, B.P. 34, Bâtiment 200, Campus d'Orsay, 91898 Orsay Cedex, France
(Received 4 October 2000; published 24 January 2001)

Typical sources of gravitational wave bursts are supernovae, for which no accurate models exist. This calls for search methods with high efficiency and robustness to be used in the data analysis of foreseen interferometric detectors. A set of such filters is designed to detect gravitational wave burst signals. We first present filters based on the linear fit of whitened data to short straight lines in a given time window and combine them in a nonlinear filter named ALF. We study the performances and efficiencies of these filters, with the help of a catalogue of simulated supernova signals. The ALF filter is the best performing and most efficient of all filters. Its performance reaches about 80% of the optimal filter performance designed for the same signals. Such a filter could be implemented as an online trigger (dedicated to detect bursts of unknown wave form) in interferometric detectors of gravitational waves.

DOI: 10.1103/PhysRevD.63.042002 PACS number(s): 04.80.Nn, 07.05.Kf

I. INTRODUCTION

Long baseline interferometric detectors of gravitational waves (GW) [1–4] will be operational in the coming years. The preparation for data analysis with these new instruments has been underway for a long time for the compact binary inspirals, the most promising source of GW to date, and for periodic sources as well (see, e.g., Ref. [5] for a review). On the other hand, it is important to develop analysis methods to search for GW bursts for which no accurate models exist. Typical sources of GW bursts are supernovae (historically the first cosmic sources of gravitational radiation ever considered). Simulations of collapses of isolated massive stars to neutron stars (type II supernovae) [6–9] suggest small departures from spherical symmetry. As a consequence, the power radiated away by GW during the few milliseconds of the collapse remains very low: the typical GW amplitude expected for such a source located at 10 Mpc does not exceed 10^{-22}–10^{-23}. This seems to give only hope for detecting supernovae events from inside our Galaxy, given the expected initial sensitivity of the current projects. The collapse of more massive stars to black holes does not seem to provide much larger amplitudes of GW [10]. One important aspect is that these simulations are unable to predict accurate wave forms for the signals, as a small change in parameters can completely change the shape of the wave form (see Ref. [8], for example). This situation calls for search methods with high efficiency and robustness against wave form variations.

Mergers of compact binaries [11] can also be considered as burst sources with perhaps good chances of detection. Some recent estimates for the amplitude of GW during the merging of two neutron stars give numbers as high as a few 10^{-21} for sources located at 10 Mpc [12]. The merging of a neutron star and and black hole seems even more efficient with amplitudes near 10^{-20} for sources at 10 Mpc [13]. The predicted amplitudes are just above the noise level of initial interferometric detectors, hence a likely detection. Note also that these two kinds of merging compact binaries are likely to be also strong emitters of gamma-ray bursts and, so, studies of coincidences between GW detectors and gamma-ray burst detectors on satellites can be crucial to validate the GW detection [14]. Here again, the details of the wave forms in the merging phase are poorly predicted. Finally, concerning the merging of two black holes, the Binary Black Hole Grand Challenge Alliance [15] intends to compute numerically the wave forms emitted during black hole collision and coalescence. Recent results suggest that GW amplitudes could also be of the order of a few 10^{-21} for a total binary mass around 10 solar masses at 10 Mpc [16].

Sources of GW bursts are then characterized by poor predictions of the emitted wave forms. At best, we only have ideas about bandwidths or typical frequencies of the signals. Matched filtering, as used for the detection of inspiraling binaries, is clearly ruled out in this case and robust methods for detecting this kind of source are then required.

Some methods have been recently proposed and studied. The ''power filter'' technique has been introduced by Flanagan and Hugues [17] in the context of binary black hole mergers, and developed further by Anderson *et al.* [18,19]. The idea here is to monitor the noise power along the time; it can be shown that this filter is optimal when only signal duration and bandwidth are known [18,19]. A similar idea (''norm filter'') has been tested independently by Arnaud *et al.* [20] to detect supernova GW signals. Time-frequency methods [21] should be also pertinent for detecting unmodelled bursts; because of their computing costs, these methods are more suited to the off-line (re-)analysis of candidates selected by faster online algorithms. Of course, one can hardly distinguish between a real burst GW signal and a transient burst caused by noise; thus methods devoted to detect nonstationarity in the noise [22] are then able to detect ''true'' signals as well. Conversely, general filters are sensitive to transient noises as well as to bursts signals. If selected by on-line triggers, these spurious events can be eliminated if they are coincident with signals detected in auxiliary sensors sensitive to different kinds of environmental noise (seismic activity, RF pickup, ...). Otherwise they can be validated when searching for coincidences between candidates from different GW detectors [23]. Furthermore, if an event is seen in coincidence by, say, the three interferometers of the Laser Interferometric Gravitational Wave Observatory (LIGO)

 ©2001 The American Physical Society

VIRGO network, then it will be possible to reconstruct the characteristics of the emitted GW signal [24]. In particular, the reconstruction of the location of the source in the sky will permit us to search for further coincidences with other types of detectors (optical telescopes or gamma-ray satellites, for example), and thus enhance the confidence level of the detection.

Our purpose is to develop and test filters for GW burst detection which are efficient, yet simple and fast enough to be used as on-line triggers [20,25,26]. In this paper, we propose to study a family of filters based on slope detection algorithms, similar to existing contour detection algorithms used for image processing, applied here to the simpler one-dimensional case. The basic idea is to detect a nonzero slope in the data stream delivered by interferometric detectors. In a first step the data are whitened by some suitable procedure [27–29], so that we assume that the noise is Gaussian and white. If we fit a finite-length time series containing only noise to a straight line, a null slope and a null offset are obtained. A nonvanishing slope could then indicate the presence of some signal added to the noise. In the following, we will first study as filters for detecting GW bursts, the two parameters of a linear fit, namely the slope (slope detector) and the offset (offset detector). These two filters are strongly correlated; it is, however, possible to decorrelate them, and finally combine them in an unique filter using the complete information. Next, we compute the performance of these filters, following a procedure already described in Ref. [20], and compare them to filters previously tested [20] and to the optimal filter taken as reference. We finally study the efficiency of the filters (fraction of events detected for a given signal over many different noise realizations).

II. SLOPE DETECTION AND RELATED FILTERS

A. The noise model

Throughout the paper, we assume that the noise is Gaussian and white with zero mean. The standard deviation of the noise is then

$$\sigma = \sqrt{\frac{S_h f_0}{2}}, \tag{2.1}$$

where f_0 is the sampling frequency and S_h is the one sided spectral density of the noise [30]. For numerical examples, we take $f_0 = 20$ kHz (VIRGO sampling rate) and $\sqrt{S_h} \simeq 4 \times 10^{-23}/\sqrt{\text{Hz}}$, which is about the minimum value of the foreseen noise spectral density of the VIRGO interferometer [31]; this choice is correct since the minimum is lying right in the frequency range for expected burst sources of GW. The fact that we choose a Gaussian noise is not essential, but simply convenient for the design of the filters. Deviation from Gaussianity will produce for example an excess in the rate of false alarms and it will then be possible to retune the algorithms according to the real noise statistics. In the frequency range of interest, above a few 100 Hz, the VIRGO noise sensitivity curve is rather flat, although not exactly white. The filtering methods presented here and in Ref. [20] require a whitening of the noise [27,28], which is foreseen for the output of the VIRGO data. In the following, we normalize the noise by its standard deviation, so that we are dealing with a Gaussian noise with zero mean and unit standard deviation.

B. Detecting a nonzero slope in the data

Let us divide the data set in sliding time windows with N samplings. Fitting the data $h(t)$ to a straight line $at+b$, we obtain the slope a and the offset b,

$$a = \frac{\langle th \rangle - \langle t \rangle \langle h \rangle}{\langle t^2 \rangle - \langle t \rangle^2}, \tag{2.2}$$

$$b = \langle h \rangle - a \langle t \rangle, \tag{2.3}$$

where $\langle x \rangle = (1/N)\Sigma_{i=1}^{N} x_i$ is defined as the arithmetic mean of the x_i in the interval of length N. Here, $t_i = i/f_0$ is the ith sampled time and h_i is the ith sampled value of the detector output. The fit transforms the input normalized Gaussian noise into Gaussian random variables, considered as linear filters, with zero mean and standard deviations σ_a and σ_b. For a linear filter such as $Y = \Sigma_{i=1}^{N} \alpha_i X_i$, the standard deviation of the filter output Y is given by $\sigma_Y^2 = \Sigma_{i=1}^{N} \alpha_i^2$, provided the X_i are normalized Gaussian variables. After a straightforward rearrangement of the above equations, we find

$$\sigma_a^2 = \frac{12 f_0^2}{N(N^2-1)}, \tag{2.4}$$

$$\sigma_b^2 = \frac{4N+2}{N(N-1)}. \tag{2.5}$$

We can finally compute the signal-to-noise ratio (SNR) for each of the two filters, as the filters' outputs divided by the filters' standard deviation: $X_a = a/\sigma_a$ and $X_b = b/\sigma_b$; we note that the only free parameter for both filters is the length of the analysis window N. In practice, their implementation is very simple and fast thanks to trivial recursive relations between filter outputs for two successive windows.

It is interesting to notice that the maximum signal-to-noise ratio (SNR) X_a or X_b with respect to the window size N is in general not obtained when the slope a or the offset b is maximum. This point is illustrated in Figs. 1 and 2, where we plot the slopes and SNR for a Gaussian burst signal $\exp[-(t-t_0)^2/2\Delta^2]$ with $\Delta = 0.5$ ms and $t_0 = 25$ ms (signal maximum at the center of the time scale). In Fig. 1, the analysis window size is $N = 10$, while in Fig. 2, it is $N = 100$. The slope computed by the fit procedure is much larger in the first case ($N = 10$) than in the second ($N = 100$) (factor about 5). Nevertheless, the SNR is higher (by a factor of about 5 in this example) for the $N = 100$ window than for the $N = 10$ window. This is due to the fact that a larger window size allows to average the effect of the noise; indeed, from Eq. (2.4), we see that σ_a^2 scales as $1/N^3$. Thus, for a Gaussian signal of width Δ, the optimal window size is found to be about $N \simeq 7\Delta/f_0$, as seen in Fig. 3. The same is observed for the offset detector (to a lesser extent) and for the derived filters described below.

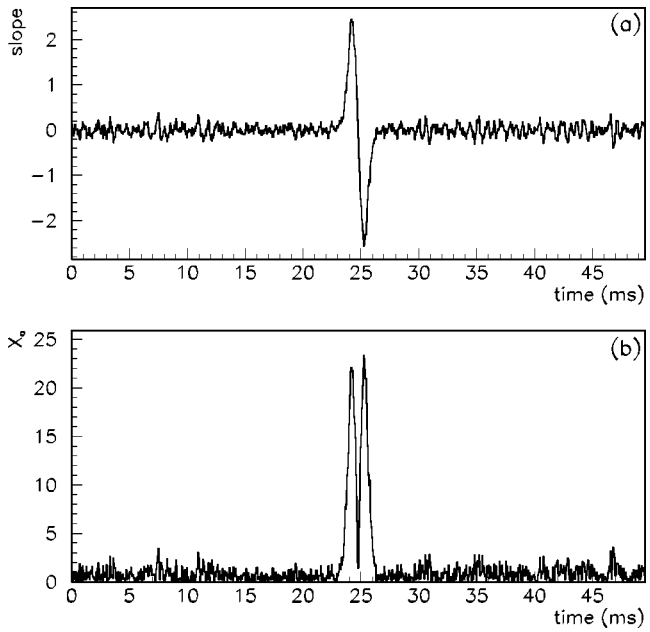

FIG. 1. Slope a (upper) and SNR X_a (lower) for a Gaussian burst signal of width $\Delta=0.5$ ms. The analysis window size is $N=10$, i.e., 0.5 ms.

C. Decorrelation of the slope and offset detectors

In case of noise alone, the normalized offset and slope detectors X_a and X_b are two highly correlated random variables. They can be decorrelated by diagonalizing the covariance matrix of X_a and X_b:

$$C=\begin{pmatrix} 1 & \alpha \\ \alpha & 1 \end{pmatrix}, \tag{2.6}$$

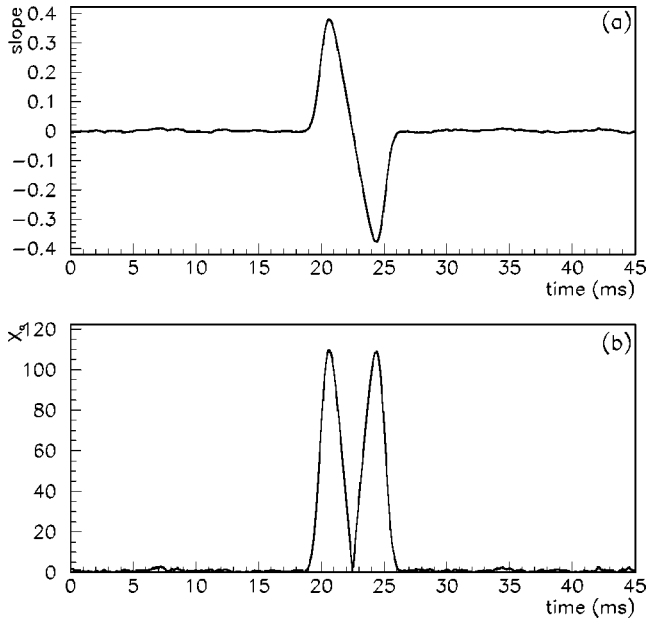

FIG. 2. Slope a (upper) and SNR X_a (lower) for a Gaussian burst signal of width $\Delta=0.5$ ms. The analysis window size is $N=100$, i.e., 5 ms.

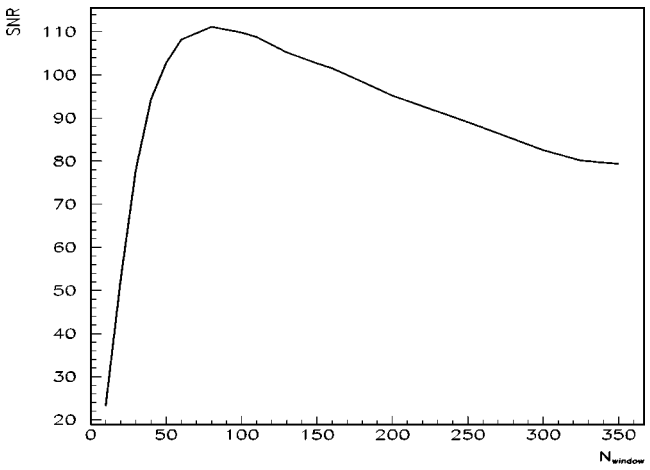

FIG. 3. SNR X_a for a Gaussian burst signal of width $\Delta=0.5$ ms as a function of the analysis window size N. The maximum SNR is obtained for $N\simeq 7\Delta$.

where $\alpha=\mathrm{cov}(X_a,X_b)$. The eigenvalues of C are then $1\pm\alpha$, corresponding to the eigenvectors $X_a\pm X_b$. Two new uncorrelated random variables are introduced:

$$X_{\pm}=\frac{X_a\pm X_b}{\sqrt{2(1\pm\alpha)}}. \tag{2.7}$$

$X_{\pm}$ are normalized in such a way that they are standard normal variables, if X_a and X_b are standard normal variables.

The computation of the covariance α is easy, yielding

$$\alpha=-\sqrt{\frac{3}{2}\left(\frac{N+1}{2N+1}\right)}. \tag{2.8}$$

The two new statistics $X_{\pm}$ can be used as uncorrelated filters for detecting GW bursts, but can also be easily combined into a unique filter.

D. The combined filter: ALF

The optimal variable retaining the full information contained in the slope and offset filters is

$$A=X_+^2+X_-^2=\frac{X_a^2+X_b^2-2\alpha X_aX_b}{1-\alpha^2}. \tag{2.9}$$

In the absence of signal in the noise, A is well approximated by a χ^2 with 2 degrees of freedom, as a sum of the square of two uncorrelated (albeit not independent) normal variables. The filter based on A is called ALF (alternative linear fit filter). Again, the only free parameter is the window size N. Note that ALF, although based on a linear fit (hence the name), is not a linear filter, contrary to the slope, offset and $X_{\pm}$ filters.

E. Threshold for detection and false alarms

1. Redefinition of an event

A major problem arises when such filters are implemented, and tested with real (or simulated) data. To be optimally efficient and because of the short durations of the signals we are interested in, each filter is applied every time step ($\delta t = 5 \times 10^{-5}$ s for VIRGO). As a consequence, a same false alarm is likely to appear for different window sizes, if different analysis windows are used in parallel, and for consecutive windows: this is the multitriggering problem.

The redefinition of an *event* solves this problem. For each window size N used in the implementation of the filters, we note t_{start} and t_{end}, the time characteristics of each triggered event (time series of data points for which SNR $\geqslant \tau$, where τ is the detection threshold). One has to take into account all the possibilities of overlapping between the different intervals. For instance, $[t_{start1}, t_{end1}]$ (for analysis window N_1) and $[t_{start2}, t_{end2}]$ (for analysis window N_2) will describe the same *event* if, e.g., $t_{start1} \leqslant t_{start2} \leqslant t_{end1}$ and $t_{end1} \leqslant t_{end2}$. Each selected event will be a cluster of points, characterized by a starting time and an ending time.

2. General discussion

We set a detection threshold by choosing a false alarm rate κ_0. In all the following numerical examples, we consider $\kappa_0 = 10^{-6}$, corresponding to 72 false alarms per hour for a 20-kHz sampling frequency. This choice results from a compromise between the necessary data reduction after online processing (the ratio reduced data/raw data should not exceed a few percent) and the weakness of the GW signals we are looking for. For instance, it will be shown in the following that, with such a false alarm rate, optimal filtering of a sample of supernovae signals gives, on average, an upper limit for the distances of detection of the order of the radius of our galaxy, using realistic simulations for the emitted waves. A large part of these false alarms will be in principle then discarded, when working afterwards in coincidence with other detectors, supposing that the different detectors noises are well uncorrelated. Obviously, this rate should be adjusted in future coincidence experiments by the maximum allowed rate for accidental coincidences. One could have chosen a false alarm rate so that the mean detection distance obtained by matched filtering of realistic supernovae wave forms corresponds to, e.g., the diameter of the Milky Way ($R \simeq 30$ kpc) or the distance of the Magellanic Clouds ($d \simeq 55$ kpc). In both cases, however, the number of false alarms is too high to be manageable (hundreds or thousands of false alarms per hour).

Anyway, the exact choice of the false alarm rate, and the corresponding threshold, is not important in this study, since we concentrate in the following on the *relative* performances of the filters (relative with respect to the optimal filter with the same false alarm rate), provided that these performances do not crucially depend on the false alarm rate. Figure 4 shows the evolution of the relative performance (see below for the accurate definition of performance) of the ALF filter averaged over a sample of realistic supernovae signals (described below) as a function of the false alarm rate. This performance shows to be relatively constant for weak false alarm rates, and begins to increase for (nonrelevant) extremely high false alarm rates ($\kappa \simeq 10^{-3}$ corresponds to several thousands of false alarms per hour); this last feature is due to the redefinition of a event, which gives a larger threshold reduction for large false alarm rates.

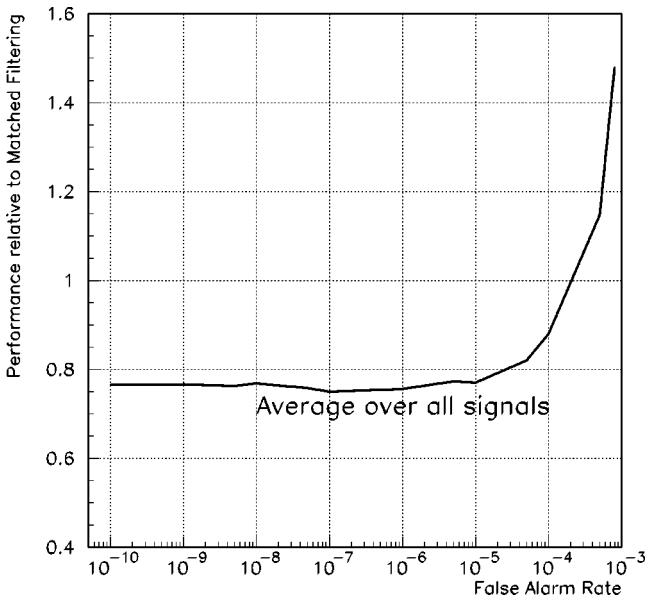

FIG. 4. Relative performance of ALF (single windowed) as a function of the false alarm rate, averaged over all the signals of the catalogue.

The false alarm rate chosen in this paper corresponds to a threshold of about $\tau \simeq 4.89$ for a normalized Gaussian variable (slope and offset detectors, X_+ and X_-) and to a threshold of about 27.63 for a two-dimensional χ^2 (ALF). This supposes of course an implementation with an unique window size; if several window sizes are to be used in parallel, then the threshold has to increased accordingly to keep the same overall false alarm rate. The actual false alarm rate is then altered by the redefinition of events that is adopted here. As an example, for a single-windowed slope detector, the same detection threshold would correspond to false alarm rate $\kappa_0 = 10^{-6}$ if the definition of an event is taken into account, and to a false alarm rate roughly equal to $2 \times \kappa_0$ if not.

3. Can we use the clustering information?

The real false alarm rate will correspond to the number of streams of data points N_i in which SNR $\geqslant \tau$ (τ is the detection threshold). The information provided by clustering can be used in two different ways.

First, for a given false alarm rate κ (corresponding to a detection threshold τ for ALF), and for a given window size, one can determine the probability P (cluster size $\geqslant n$) for a cluster of size larger than n to occur. A cluster of size larger than n will then be found with a rate $\kappa \times P(n)$. An integer n_0 can be found such that $\kappa \times P(n_0) = \kappa_0$. As a consequence, the detection threshold τ for ALF corresponding to κ will be lowered. The definition of an event in this case will thus be a cluster of size $\geqslant n_0$ for which SNR $\geqslant \tau$. The results obtained

with such a definition are similar to the ones described in the next section.

The distribution of the number of consecutive triggers for a given threshold can be used in another way. This distribution gives a probability of occurrence $P(n)$ of a given number n of consecutive triggers for the fixed threshold τ. Then, each cluster can be labeled with the corresponding probability, and one can put *priority* in the treatment of those events. Furthermore, putting a threshold on the quantity n can help to remove some of the false alarms. In this case, one can hope to discard a substantial part of the events, which with great probability are actually false alarms. Of course, the loss of signal this process causes has to be quantified. For high SNR's physical signals, using ALF, an average loss as high as 20% is observed for a 50% false alarms removal. The price to pay for such a removal is clearly too high.

III. DETECTION OF SUPERNOVAE

In order to benchmark the filters, we use a catalogue of simulated supernova GW signals. Indeed, as we need ''robust'' filters with respect to the details of the wave forms, it seems convenient to average the filters performances over a variety of (physically sound) wave forms.

A. The catalogue of signals

As in Refs. [26] and [32], we use as a catalogue the 78 GW signals simulated by Zwerger and Müller [8] which are available in Ref. [33]. These wave forms result from the collapse of massive stars into neutron stars within the assumption of axial symmetry. The fact that the collapses are axially symmetric is unimportant for our studies which require only a set of (as physically sound as possible) burst signals with a variety of wave forms in order to test the filters' robustness against the current poor knowledge of the burst wave forms. Each signal corresponds to a particular set of parameters, mainly the initial distribution of angular momentum inside the progenitor star and the rotational energy in the core. All the signals are computed for a source located at 10 Mpc; we can then re-scale the amplitudes of wave forms in order to locate the source at any distance. In the following, we assume that the incoming wave forms are optimally polarized, along the interferometer arms; this assumption has no consequence on the relative performances of the filters. The detection distances displayed below have then to be considered as upper limits. Zwerger and Müller distinguish three different types of wave forms. Type I signals typically present a first peak (associated to the bounce) followed by a ring down. Type II signals show a few (2–3) decreasing peaks, with a time lag between the first two of at least 10 ms. Type III signals exhibit no strong peak but fast ($\sim$1 kHz) oscillations after the bounce.

As the wave forms in the catalogue are explicitly known, optimal filtering can be used as a benchmark. The optimal SNR ρ_0 for a GW signal $h(t)$ (e.g., any of the 78 signals in the catalogue, located at a distance d) is given by

$$\rho_0^2 = 2\int \frac{|\tilde{h}(f)|^2}{S_h(f)} df = \frac{f_0}{\sigma^2}\int |h(t)|^2 dt, \tag{3.1}$$

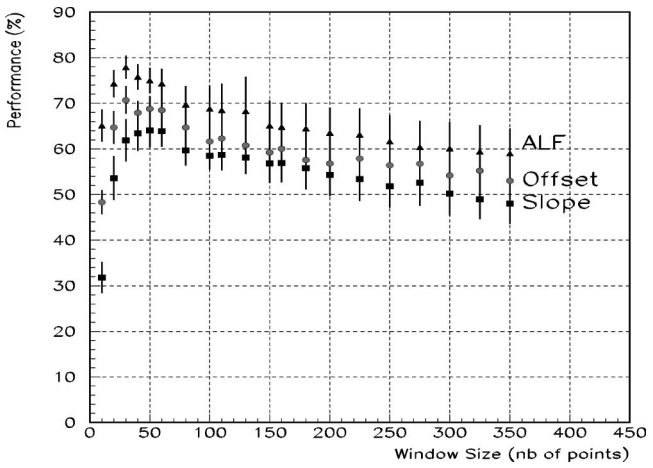

FIG. 5. Performance of single-windowing filters slope, offset, and ALF as a function of the window size. The error bars take into account the finite statistic of the wave forms taken from the catalogue.

where we use the relation between the one-sided spectral density of the noise S_h, the sampling frequency f_0, and the r.m.s of the noise σ given by Eq. (2.1). Since the noise is whitened in the detection bandwidth, S_h is constant and the Parseval's theorem can be used. The optimal SNR ρ_0 is proportional to $\langle 1/d \rangle$. We can rather define a (mean) distance of detection as the distance for which the signal is just detected, that occurring when ρ reaches the threshold τ. Such mean detection distances have to be found by simulations (because $\langle d \rangle$ is always larger than $\langle 1/d \rangle^{-1}$). With $\tau \simeq 4.89$, we obtain a distance of detection, averaged over the N_c signals of the catalogue (here $N_c = 78$), $d_0 = (1/N_c)\Sigma_{i=1}^{N_c} d_0^{(i)} \simeq 26.5$ kpc, where $d_0^{(i)}$ is the optimal distance of detection for the ith signal of the catalogue. We note that, with the threshold we have chosen, d_0 is of the order of the diameter of our Galaxy; a few signals (those with large initial rotational energy) have optimal distances of detection larger than 50 kpc, the distance to the Large Magellanic Cloud. The largest distance of detection obtained in the sample is about 130 kpc.

B. Definition of the performance

Let us consider the ith signal in the Zwerger and Müller catalogue. Its mean optimal distance of detection, defined above, is $d_0^{(i)}$. The mean distance of detection obtained with another filter is $d^{(i)}$ (averaged over noise realizations). We then define the performance of the filter for this signal as $d^{(i)}/d_0^{(i)}$. This relative definition is convenient, because of the different ''strengths'' of the signals in the catalogue. The global performance Π of the filter is then defined as the average of the performances for the N_c signals of the catalogue:

$$\Pi = \frac{1}{N_c}\sum_{i=1}^{N_c} \frac{d^{(i)}}{d_0^{(i)}}. \tag{3.2}$$

Figure 5 shows the performances of the slope and offset detectors and of ALF, as a function of the window size. The

TABLE I. Optimal analysis window sizes and performances. The performance is averaged over the 78 signals for all filters, with one single window size for all signals.

Filter	SD	OD	ALF
Optimal window size (ms)	2.5	1.5	1.5
Performance	0.65	0.70	0.78

maximal performances are obtained for small window sizes (between 20 and 40 bins, that is, 1 ms and 2 ms). The slope detector (SD) has a performance greater than 0.6 for window sizes (N_w) up to 100 bins (5 ms). The offset detector (OD) keeps a performance greater than 0.6 up to $N=7.5$ ms while the performance of ALF is always greater than 0.6 up to $N \simeq 17$ ms. For all the window sizes studied here, all the filters have performances greater than 0.5. For X_+ and X_- (not shown in Fig. 5), the maximal performances are $\Pi_{\max} \simeq 0.71$ and $\Pi_{\max} \simeq 0.67$. The ALF, which combines the informations of the slope and offset detectors, is the best performing for any window size (see Table I).

C. Window size and detection strategy

In fact, each of the signals will be optimally detected with a given analysis window size N_i (for signal i). The distribution of those window sizes for all Zwerger and Müller (ZM) signals (see Fig. 6) shows different ''preferred'' regions. If each signal was detected with its own optimal window size (unrealistic case), the overall performance could rise to 0.91 for ALF. In fact, to stay as unbiased as possible, it is possible to discretise the window size parameter space, allowing, for example, 5, 10, or 20 different window sizes used for the same filter. The size of windows and their spacing is not crucial for a given number of window, as the performances of the filters do not depend crucially on these parameters (within typically 1%).

Of course, the individual threshold for each of the window sizes would have to be higher in order to obtain an *overall* false alarm rate (taking into account the redefinition of a false alarm) equal to 10^{-6}.

D. Performances of the filters

Table II shows the performances obtained with multiwindowing slope, offset and ALF filters, using $\{\text{window sizes}\} = \{1.5, 2.5, 5, 10, 15 \text{ ms}\}$ (with a clear preference for short duration windows).

We recall also the performances of the norm filter (NF) and the peak correlator (PC) [20,30]. The peak correlator is implemented with 26 (truncated) Gaussian templates of widths optimally located in the interval [0.1, 10 ms]. All filters related to the slope detector excepted ALF have performances from 0.5 up to about 0.7, while ALF reaches a performance greater than 0.8.

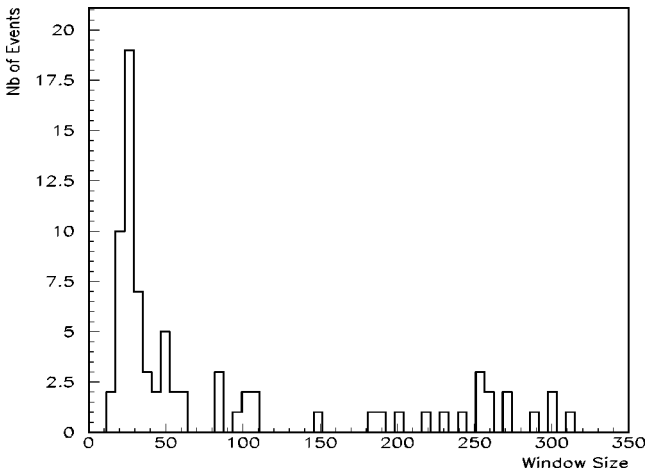

FIG. 6. Distribution of window sizes (in number of samplings at 20 kHz) that give optimal performances for ALF. Short duration windows (up to about 100 bins, i.e., 5 ms) are clearly preferred.

It has been noticed that with 20 window sizes (rather than 5) in parallel, all filters related to ALF have performances around 0.8. Indeed, to keep an overall false alarm rate of κ_0 for n_{window} window sizes in parallel, the individual false alarm rate to apply for each window size is roughly given by κ_0 / n_{window}. This quantity is then tuned by simulations, because each of the filters studied here react in a different way with respect to the event redefinition. The fact that $\Pi_{ALF}^{5\ windows} \simeq \Pi_{ALF}^{20\ windows}$ whereas $\Pi_{L}^{5\ windows} < \Pi_{L}^{20\ windows}$ (where L denotes all the linear filters, i.e., all the filters except ALF) shows the robustness of ALF with respect to a variation of the detection threshold.

E. Robustness of performances with respect to signal type

Table III shows the mean performances of the filters described above for each of the three types of signal in the ZM catalogue. Each of the filters are nearly equally performant with type III signals, except X_+ and ALF which show much better performance. They all seem to have the same behavior for type I signals, whereas great differences can be seen in their performances with type II signals (from 0.46 for SD to 0.72 for X_+).

ALF shows its best performances for type III signals (short durations and high frequencies), whereas types I are preferred by SD and X_-, and type II by OD and X_+. Those results give a dispersion (with respect to signal type) of about 5% for all filters.

TABLE II. Performances of the ALF and related filters, each implemented with five windows in parallel.

Filter	Optimal	NF	PC	SD	OD	X_+	X_-	ALF
Average distance (kpc)	26.5	11.5	18.5	11.3	15.2	18.4	13.1	22.5
Performance (%)	1	0.46	0.73	0.49	0.59	0.66	0.54	0.81

TABLE III. Performances (in percent) of the ALF and related filters. Each filter is implemented with five windows applied in parallel on the different kinds of signals of the ZM catalogue.

Filter	SD	OD	X_+	X_-	ALF
Type I signal performance	0.53	0.60	0.59	0.57	0.79
Type II signal performance	0.47	0.62	0.72	0.54	0.81
Type III signal performance	0.41	0.48	0.62	0.45	0.89

Concerning the robustness of the filters, one could argue that we have studied the performance of the filters with only one set of GW signals. It is worth noting that the linear fit filters have been also tested on other ''signals'' than those given by the Zwerger and Müller catalogue: generic peaks or damped sine [32]. This kind of signal could be the signature of typical instrumental artifacts but also of real GW signals such as black hole oscillations [34], for example. The performances in this case are similar (or better) to the benchmark above, except in the case of high frequency (kHz) and slightly damped signals (long signals), where the performance of ALF, for example, falls down to about 0.3, while it is close to 1. for very short bursts (Gaussian peaks and strongly damped sine as well).

F. Efficiency of the filters

Another way to compare the different filters is to compute their efficiency as a function of the distance of the source. The efficiency for a given signal located at a given distance is defined as the number of detections over the total number of simulated noise realizations. Again the efficiency is there calculated by averaging over the signals of the ZM catalogue. Figure 7 presents the detection efficiency for the different filters, SD, OD, and ALF as a function of the distance to the source, expressed in units of the optimal distance of detection for this particular source, and averaged over all the signals. That means that each source has been located to a distance $x \times d^i_{optimal}$, where $d^i_{optimal}$ is the mean detection distance obtained with the matched filtering for the ith signal in the catalogue, and $x \in [0,1]$. The detection efficiency presented here is the mean of the detection efficiencies obtained for each signal in the catalogue. X_- (not shown in Fig. 7) behaves like OD at small distances and like SD at larger distances (this is the contrary for X_+).

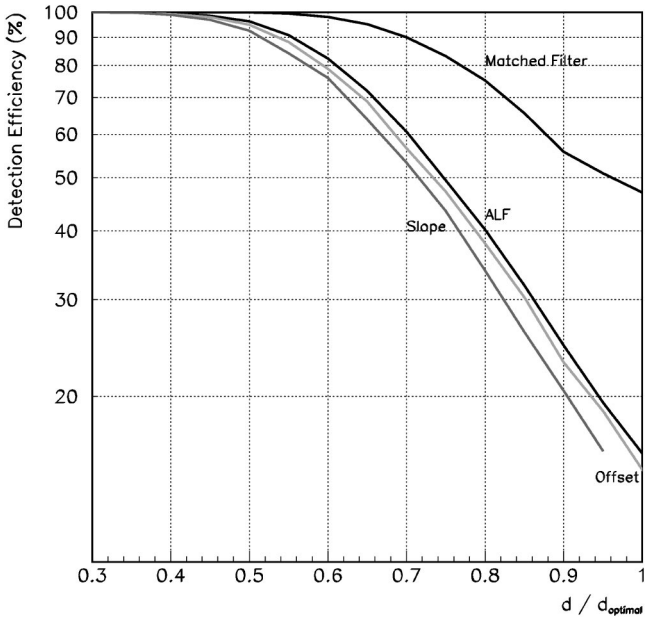

FIG. 7. Detection efficiency of the filters as a function of the distances of the source. The distances are normalized to the optimal distances of detection for each signal and the efficiency is averaged over all the signals of the Zwerger and Müller catalogue.

We can also derive the distances d_e for which each signal reaches a efficiency of e% (see Table IV). We note that in spite of performances rather different for all the filters presented here, their detection efficiencies behave quite similarly. Eventually, all filters have the same *effective performance* Π_{eff} defined by $d_{50}/d_{\text{optimal}}$, which is around 0.75. We note also that the efficiency of the Wiener filter is around 50% for the optimal distance of detection $d/d_{\text{optimal}}=1$. Figure 8 shows the false dismissal rate (ratio of missed events or *inefficiency*) as a function of the false alarm rate, for signals located at 10 and 25 kpc, for a single windowed ALF filter. At 10 kpc, with realistic false alarm rates (of the order of 10^{-6}–10^{-7}), the dismissal rate is about 40–50 %. Small dismissal rates can be reached with extremely high false alarm rates (greater than 10^{-3}). Even if the performances of such a filter seems to be very high, the detection of sources (from such a catalogue) out of our Galaxy will be clearly difficult. The last curve (labeled d_{95}) shows the evolution of the false dismissal rate where each signal of the catalogue has been located to a distance at which, for final ALF (five windows), the detection efficiency is 95%. This means that in this case, each source is located at the same fraction of its own optimal detection distance (hence a *different* distance for each source).

IV. SENSITIVITY OF THE FILTERS TO NONWHITE NOISE

It is likely that the data provided by the interferometric detectors will be non-Gaussian and nonwhite. On-line filters

TABLE IV. Average source distances for which the ALF and related filters reach a 95% (50%) efficiency.

Filter	Optimal	SD	OD	X_+	X_-	ALF
$d_{95}/d_{\text{optimal}}$	0.65	0.47	0.5	0.47	0.49	0.52
$d_{50}/d_{\text{optimal}}$	0.96	0.72	0.73	0.72	0.73	0.75

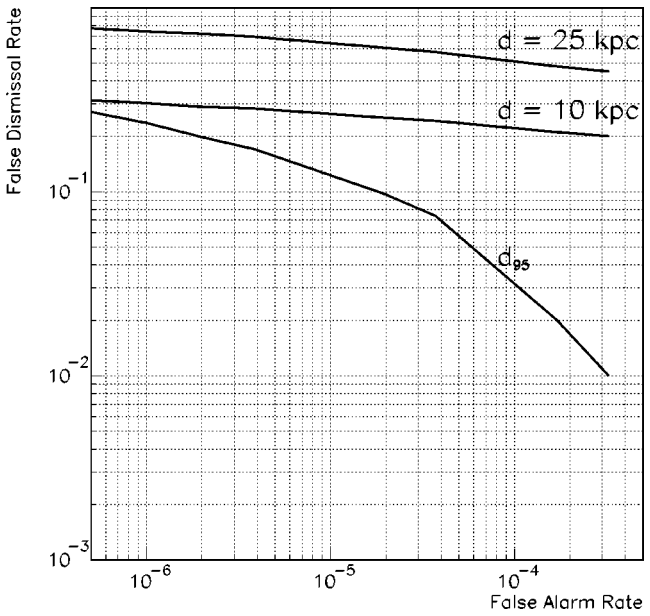

FIG. 8. False dismissal rate as a function of false alarm rate for all signals located at 10 and 25 kpc. The curve labeled d_{95} concerns signals located at a distance such that for ALF (with five different window sizes), $\epsilon_{ALF} \simeq 95\%$ (for $\kappa_0 \sim 10^{-6}$), that is, a *different* distance for each signal. Dashed lines represent 25, 50, and 75 % false dismissal rate.

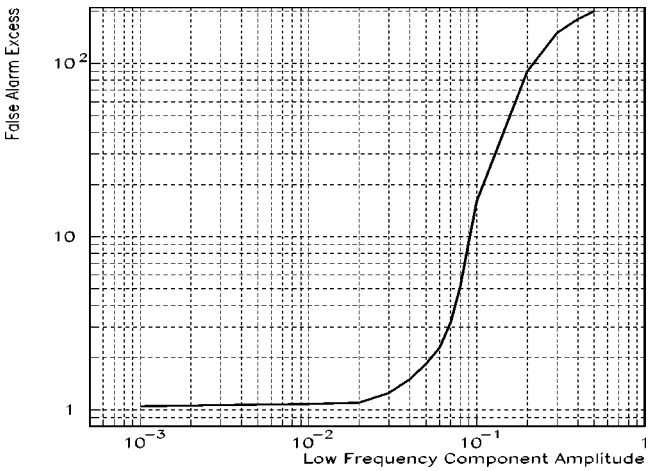

FIG. 9. False alarms excess as a function of the amplitude of a low frequency component (here 0.6 Hz) added to white noise. This excess is the quantity (effective number of false alarms)/(allowed number of false alarms). The amplitude is measured relatively to the standard deviation of the noise. In this figure, the amplitude $A_{10\%}$ represents a false alarm excess of 1.1.

will process prewhitened data, and this whitening will be certainly nonperfect. This is a crucial point to know how online triggers will behave in such a case. In order to study this effect, we thus have added to the white Gaussian noise low frequency components of the type $A_{bf} \sin(2\pi ft)$. We then compute, as a function of the frequency f, the amplitude $A_{10\%}$ which corresponds to an increase of 10% of the number of false alarm, for the final multiwindowing ALF filter.

For $f = 0.6$ Hz (pendulum mode in VIRGO), we find that the maximum authorized amplitude is of the order of $2 \times 10^{-2} \times \sigma_{noise}$. For other frequencies, $A_{10\%}$ is in the range 2×10^{-2}–5×10^{-2} ($\times \sigma_{\rm noise}$) up to 1 kHz. Figure 9 shows the evolution of the false alarms excess as a function of the amplitude of the 0.6-Hz component in imperfectly whitened samples of data. A low frequency amplitude about five times larger than $A_{10\%}$ for $f = 0.6$ Hz gives ten times more false alarms. This proves (if needed) that the whitening process will be a crucial part of the analysis procedure.

V. CONCLUSIONS

We have designed and tested some filters based on linear fits and aimed at the detection of short bursts of gravitational waves, such as the ones emitted by massive star collapses. In particular, we have built a nonlinear filter, ALF, from the slope and offset detectors resulting from the fit procedure. These filters match the simplicity and speed requirements needed for on line triggers to be easily implemented in interferometric detectors of gravitational waves. The performances of the filters are better than those of the filters studied in Ref. [20] with the same procedure. In particular, the ALF filter, if implemented with five windows, reaches a performance of about 80%, relative to the matched filter, and the detection efficiency for such signals is about 50% at a distance $d \sim 0.75 \times d_{\rm optimal}$. This is, however, just enough to detect supernova signals from anywhere in the Galaxy. Indeed, the mean distance of detection averaged over the supernova signals contained in the Zwerger and Müller catalogue is about 22.5 kpc, of the order of the diameter of the Galaxy. This figure has been obtained by assuming an optimal incidence of the (''+'' polarized) signals along the arms of the interferometric detector, and should be in fact corrected for the incidence effect. Averaging over all the possible source locations in the sky reduces the signals by at least $1/\sqrt{5}$ (in the isotropic case). This finally results in a mean distance of detection of about 10 kpc. Clearly, with the low expected rate of supernovae in our galaxy (about three per century) massive star collapses are not likely to be detected with the first generation of interferometric detectors, unless the asymmetry of the collapse is much larger than presently expected in current models. Unfortunately, simulations of nonaxisymmetric collapses do not provide GW amplitudes much larger than in the axisymmetric case [7,9]

It is not impossible, however, that the first generation detectors could be sensitive to binary mergers as far as the VIRGO cluster (especially black hole mergers). Indeed, rough estimates of the amplitudes of the GW signals are two or three orders of magnitude larger than the ones predicted for the supernova signals; this gives crudely distances of detection that might be as large as 10 Mpc with the present detectors, LIGO I and VIRGO. Regarding the detection of GW emitted by a binary system, combining the traditional method of matched filtering for the inspiral phase and a ''pulse'' detection technique, such as those developed in this paper and in Refs. [20,25] and [26], could help to increase the final signal to noise ratio and then the confidence in the detection of an interesting event. This can be valuable especially for binary black holes, for which only a few cycles can

span the detector bandwidth, so that the contribution of the merging phase to the total signal to noise ratio can be important (see Ref. [35] for an idea of the respective strengths of the inspiral and merger wave forms).

Finally, a filter such as ALF seems to satisfy all requirements to be implemented as part as on line trigger dedicated to detect bursts of unknown wave form in interferometric detectors of gravitational waves.

[1] A. Abramovici, W.E. Althouse, R.W.P. Drever, Y. Gürsel, S. Kawamura, F.J. Raab, D. Shoemaker, L. Sievers, R.E. Spero, K.S. Thorne, R.E. Vogt, R. Weiss, S.E. Whitcomb, and M.E. Zucker, Science **256**, 325 (1992).

[2] B. Caron *et al.*, Nucl. Phys. B (Proc. Suppl.) **54**, 167 (1997).

[3] K. Danzmann *et al.*, in *Gravitational Wave Experiments*, edited by E. Coccia, G. Pizzella, and F. Ronga (World Scientific, Singapore, 1995).

[4] K. Kuroda, in *Gravitational Waves: Sources and Detectors*, edited by I. Ciufolini and F. Fidecaro (World Scientific, Singapore, 1997).

[5] B.F. Schutz, in *The Detection of Gravitational Waves*, edited by D.G. Blair (Cambridge University Press, Cambridge, England, 1991).

[6] R. Mönchmeyer, G. Schäfer, E. Müller, and R.E. Kates, Astron. Astrophys. **246**, 417 (1991).

[7] S. Bonazzola and J.-A. Marck, Astron. Astrophys. **267**, 623 (1993).

[8] T. Zwerger and E. Müller, Astron. Astrophys. **320**, 209 (1997).

[9] M. Rampp, E. Müller, and M. Ruffert, Astron. Astrophys. **332**, 969 (1998).

[10] R.F. Stark and T. Piran, Phys. Rev. Lett. **55**, 891 (1985).

[11] K. Oohara and T. Nakamura, in *Relativistic Gravitation and Gravitational Waves*, edited by J.-A. Marck and J.-P. Lasota (Cambridge University Press, Cambridge, England, 1997).

[12] M. Ruffert and H.-Th. Janka, Astron. Astrophys. **338**, 535 (1998).

[13] H.-T. Janka, T. Eberl, M. Ruffert, and C.L. Fryer, Astrophys. J. Lett. **527**, L39 (1999).

[14] L.S. Finn, S.D. Mohanty, and J.D. Romano, Phys. Rev. D **60**, 121101 (1999).

[15] The Binary Black Hole Grand Challenge Alliance's web page is located at http://www.npac.syr.edu/projects/bh/

[16] G. Khanna, R. Gleiser, R. Price, and J. Pullin, New J. Phys. **2**, 3 (2000).

[17] E.E. Flanagan and S.A Hughes, Phys. Rev. D **57**, 4535 (1998).

[18] W.G. Anderson, P.R. Brady, J.D.E. Creighton, and E.E. Flanagan, Int. J. Mod. Phys. D **9**, 303 (2000).

[19] W. G. Anderson, P. R. Brady, J. D. E. Creighton, and E.E. Flanagan, Phys. Rev. D (to be published), gr-qc/0008066.

[20] N. Arnaud, F. Cavalier, M. Davier, and P. Hello, Phys. Rev. D **59**, 082002 (1999).

[21] W.G. Anderson and R. Balasubramanian, Phys. Rev. D **60**, 102001 (1999).

[22] S.D. Mohanty, Phys. Rev. D **61**, 122002 (2000).

[23] J.D.E. Creighton, Phys. Rev. D **60**, 021101 (1999).

[24] Y. Gürsel and M. Tinto, Phys. Rev. D **40**, 3884 (1989).

[25] N. Arnaud, F. Cavalier, M. Davier, P. Hello, and T. Pradier, to appear in the proceedings of the XXXIVth Rencontres de Moriond on ''Gravitational Waves and Experimental Gravity,'' Les Arcs, 1999, gr-qc/9903035.

[26] T. Pradier, N. Arnaud, M.-A. Bizouard, F. Cavalier, M. Davier, and P. Hello, Int. J. Mod. Phys. D **9**, 309 (2000).

[27] M. Beccaria, E. Cuoco, and G. Curci, *Adaptive Identification of VIRGO-like noise spectrum*,'' in the Proceedings of the Second Edoardo Amaldi Conference on Gravitational Waves, Edoardo Amaldi Foundation series Vol. IV, edited by E. Coccia, G. Pizzela, and G. Veneziano (World Scientific, Singapore, 1998).

[28] E. Cuoco, ''Whitening of noise power spectrum,'' VIRGO note VIR-NOT-FIR 1390 145, 2000.

[29] E. Cuoco (in preparation).

[30] The $\sqrt{2}$ factor forgotten in Ref. [20] has been here corrected for.

[31] The ''official'' VIRGO sensitivity curve is available at http://www.pg.infn.it/virgo/presentation.htm

[32] F. Cavalier, M. Davier, P. Hello, and T. Pradier, ''Triggers for the detection of impulsive sources of gravitational waves,'' VIRGO note VIR-NOT-LAL-1390 128 (1999), unpublished. T. Pradier *et al.* ''Improved slope filters for detecting bursts,'' VIR-NOT-LAL-1390 160 (2000).

[33] http://www.mpa-garching.mpg.de/~ewald/GRAV/grav.html

[34] F. Echeverria, Phys. Rev. D **40**, 3194 (1989).

[35] A. Buonanno and T. Damour, Phys. Rev. D **62**, 064015 (2000).